

Fabrication of NiO/palygorskite Composite and Its Pseudocapacitance Performances

Mingjin Li^{1,*}, Aiping Li², Haiqing Xu², Liangdong Feng^{2,3,*}

¹Department of Electromechanical Engineering, Huaian College of Information Technology, Huaian 223003, PR China

²Key Laboratory for Palygorskite Science and Applied Technology of Jiangsu Province, Department of Chemical Engineering, Huaiyin Institute of Technology, Huaian 223003, PR China

³Jiangsu Provincial Key Laboratory for Interventional Medical Devices, Huaian 223003, PR China

*E-mail: lmj_hcit@163.com or ldfeng@hyit.edu.cn

Received: 29 January 2015 / Accepted: 20 February 2015 / Published: 23 March 2015

NiO/palygorskite composites had been fabricated by combining hydrothermal and calcining methods. The structure, morphology, surface area and pore distribution of the as-prepared NiO/palygorskite composites were characterized by the techniques such as powder X-ray diffraction (XRD), scanning electron microscopy (SEM), transmission electron microscopy (TEM), energy-dispersive X-ray spectrum (EDS) and Brunauer-Emmett-Teller (BET). The synthesized NiO/palygorskite composite had larger BET surface area of 129.2 m²/g. The obtained NiO/palygorskite composites showed high specific capacitance of 1085.3 F/g at current density of 0.25 A/g.

Keywords: NiO/palygorskite composite, fabrication, pseudocapacitance

1. INTRODUCTION

Recently, great success has been achieved using NiO as a pseudocapacitor electrode material due to its large surface area, high pseudocapacitance behavior and low cost. So far, diverse NiO nanostructures have been fabricated and exhibited quite encouraging pseudocapacitive performance [1-17]. The pseudocapacitance of nickel oxides is influenced by its material parameters, such as the structure, conductivity and crystallinity, electrolyte, and material loading mass on the electrode [18]. For example, the specific capacity (C_s) of nickel oxides can be greatly influenced by their structure including morphology, size, specific surface area, pore size and distribution, and the morphology is closely related to the specific surface area. Unfortunately, not all of the surface area of NiO is electrochemically accessible by the electrolyte, so, the C_s of NiO is not a linear function of its specific

surface area. The capacity of NiO strongly depends on the surface area of the electrode accessible to the electrolyte [19, 20].

In order to improve the pseudocapacitance of nickel oxides, nickel oxides with different structures have been fabricated and their capacitive properties have been investigated by different electrochemical methods. For example, Li *et al.* have prepared mesoporous NiO network-like hierarchical microspheres with ultrathin nanowires, this material could deliver a C_s value of 555 F/g at a current density of 2 A/g, which was benefit to the unique hierarchical NiO architectures with appropriate pore size and surface texture, and a high specific surface area [10]. Zhang *et al.* have grown various porous NiO nanostructures including nanoslices, nanoplates, and nanocolumns, which showed a structure-dependence in their specific charge capacitances. The specific surface areas were determined to be 102.4, 20.2, and 11.4 m²/g for the nanocolumns, nanoplates, and nanoslices, and the corresponding specific capacitance at a discharge current of 5 A/g were 390, 285 and 176 F/g, respectively [2]. A hierarchically porous NiO film with a structure consisting of NiO triangular prisms and randomly porous NiO nanoflakes, possessed a total specific surface area of 196.8 m²/g, exhibited a high discharge capacitance of 232 F/g at a current density of 2 A/g [7]. A three-dimensional nanoporous NiO film with highly nanoporous structure and high surface area of 264 m²/g were prepared by Hu's group, the material showed a high specific capacitance of 1776 F/g at a scan rate of 1 mV/s [9].

Despite the progress in enhancing the C_s value of nickel oxides through fabricating materials with different morphologies, sizes, surface areas and pore size distributions, single-phase NiO electrodes are found to have unsatisfactory performance because of their intrinsic weaker material properties in conductivity, cycling stability and mechanical stability [21]. So, different materials such as carboneous materials, metals, transition metal oxides, or hydroxides have been adopted to form NiO composite electrodes with synergistically optimized performances. In practice, the nano sized NiO are easily agglomerated, and decrease its specific surface area and number of reactive sites, which thereby reduce its capacitance performance. We hope that the combination of nickel oxide nanoparticles and materials with high specific surface area can reduce the agglomeration of NiO particles and thus increase the specific surface area and number of reactive sites, with a corresponding improvement in capacitance performance. Palygorskite, a species of hydrated magnesium aluminum silicate mineral, was characterized by a porous structure with commonly fibrous morphology. Due to its high specific surface area and high adsorption capacity, palygorskite has been widely used as an adsorbent, catalyst, and catalyst support [22 - 24].

Herein, we describe a facile hydrothermal preparation of NiO/palygorskite composite. The resulting composites were characterized in detail using X-ray diffraction (XRD), scanning electron microscopy (SEM), transmission electron microscopy (TEM) and Brunauer-Emmett-Teller (BET) techniques. The pseudocapacitive performance of the composite was also investigated by cyclic voltammetry (CV), chronopotentiometry (CP) and electrochemical impedance spectroscopy (EIS) measurements.

2. EXPERIMENTAL

2.1. Materials preparation

Analytical grade of nickel acetate tetrahydrate ($C_4H_6O_4Ni \cdot 4H_2O$), urea ($CO(NH_2)_2$) and potassium hydroxide (KOH) were purchased from Shanghai Chemical Reagent Co. Palygorskite (99.9%) was purchased from Jiuchuan clay company (Jiangsu, China). All reagents were used without further purification, and distilled water was used throughout.

NiO nanotubes were prepared as follows: firstly, 1 wt% palygorskite suspended solution was prepared and stirred using a magnetic agitator for 1.0 hours. Then, 1.0 g of $C_4H_6O_4Ni \cdot 4H_2O$ was dissolved in 40 mL of 1 wt% palygorskite solution and stirring for 0.5 hours, after that, 0.96 g of $CO(NH_2)_2$ was dissolved in the above solution. The solution was placed in a 50 mL Teflon-sealed autoclave and maintained at 120 °C for 24 hours. The products were filtered, washed with distilled water and ethanol for three times, respectively, and dried at 80 °C for 24 hours, the obtained products were marked as $Ni(OH)_2$ /Palygorskite composite. Finally, a subsequent calcination process was carried out at 350 °C for 6 hours, and the final products were NiO/palygorskite composites. For comparison, NiO nanoparticles were prepared by the same method.

2.2. Characterization

The crystallinity of the products were analyzed by a Bruker D8 Advance X-ray diffractometer at a scanning rate of 4°/min using Cu K α radiation ($\lambda = 0.15406$ nm). Multipoint nitrogen adsorption/desorption curves were recorded on an automatic Micromeritics Tristar II 3020 analyzer using Brunauer-Emmett-Teller (BET) gas adsorption method at 77 K. All samples were outgassed at 100 °C for 6 h under flowing nitrogen before measurements. The specific surface area values were calculated using the software of the instrument based on BET equation. Pore size and pore size distribution plots were obtained by Barrett–Joyner–Halenda (BJH) method using the cylindrical pore model. The SEM images were carried out on a Quanta 250 FENG field-emission scanning electron microscopy (FESEM, FEI) with Energy dispersive spectrometry (EDS, Oxford UK). TEM analysis was conducted on a Tecnai 12 electron microscope (Philips, Holland) operated at 120 kV. A model Optima 7000 (Perkin-Elmer, USA) ICP-OES was used as the measurements.

Electrochemical experiments were carried out on a CHI 660C electrochemical workstation (Chenhua, Shanghai, China) at room temperature. A traditional three electrode configuration was used with NiO/palygorskite coated nickel foam sheet as the working electrode, A platinum foil (1×2 cm²) and HgO/Hg (1.0 mol/L KOH) served as counter electrode and reference electrode, respectively. The working electrodes were prepared by mixing the obtained NiO/palygorskite composite with 5 wt% polytetrafluoroethylene and 20 wt% acetylene black of the total electrode mass. A small amount of ethanol was added to this composite to make a more homogenous mixture, which was pressed on nickel foam sheet, and vacuum-dried at 60 °C for 8 h. All potentials given below were relative to the HgO/Hg.

CV, CP and EIS studies were performed in a 2.0 mol/L KOH deoxygenated aqueous. The electrochemical impedance spectra were measured by imposing a sinusoidal alternating voltage frequency of 1×10^{-2} to 1×10^5 Hz with amplitude of 5 mV at constant dc bias potential of 0.5 V.

3. RESULTS AND DISCUSSION

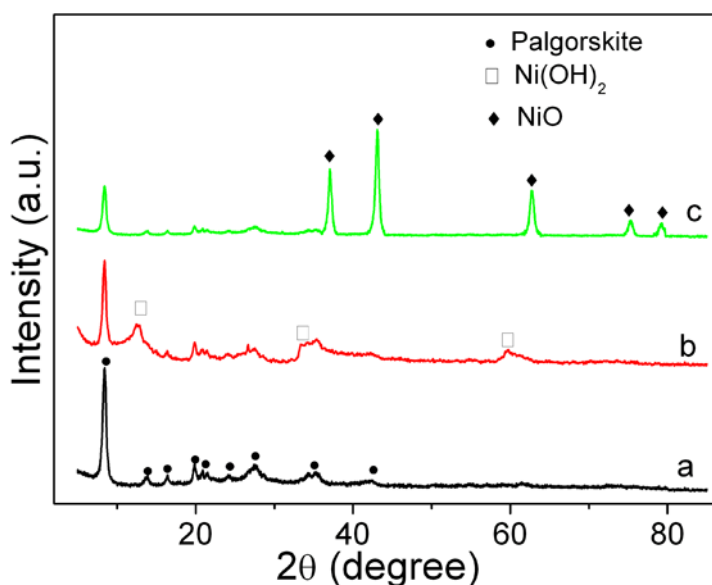


Figure 1. XRD patterns of palygorskite (curve a), Ni(OH)_2 /palygorskite (curve b) and NiO /palygorskite composite (curve c).

The structure and phase analysis of the samples were performed by powder XRD technique, and the results were shown in Fig. 1. Most of the peaks in the XRD patterns of palygorskite (curve a) can be assigned to monoclinic palygorskite ($a = 17.86 \text{ \AA}$, $b = 12.68 \text{ \AA}$, $c = 5.127 \text{ \AA}$ and $\beta = 92.23^\circ$, JCPDS Card No. 29-0855). The typical peak at $2\theta = 8.54^\circ$ was attributed to the basal plane of the palygorskite structure, and the peaks at $2\theta = 13.9, 16.4, 34.4$ and 35.3° represented the Si–O–Si crystalline layers in the clay. Additionally, the peak scanned at $2\theta = 19.8$ and 27.8° could be ascribed to the quartz impurity, and the peak was also present in the Ni(OH)_2 /palygorskite and NiO /palygorskite composites. In the XRD patterns of Ni(OH)_2 /palygorskite composite (curve b), the peak at $2\theta = 8.54^\circ$ did not exhibit a considerable difference from the palygorskite. New signals at 2θ values of $12.5, 35.0$ and 59.7° could be assigned to hexagonal symmetry of $\alpha\text{-Ni(OH)}_2 \cdot 0.75\text{H}_2\text{O}$ ($a = 3.08 \text{ \AA}$ and $c = 23.41 \text{ \AA}$, JCPDS Card No. 38-0715). After calcining, the NiO crystal phase was expected to be formed, which was confirmed in curve c. The presence of NiO in the composites was confirmed by the corresponding characteristic reflection peaks at $37.2^\circ, 43.2^\circ, 62.8^\circ, 75.3^\circ$ and 79.3° assigned to the (111), (200), (220), (311) and (222) reflections of cubic NiO ($a = 4.176 \text{ \AA}$, JCPDS Card No. 78-0643), which demonstrated the successful formation of NiO phase on the palygorskite nanofiber surfaces.

The elemental composition of the obtained NiO/palygorskite composites was detected by ICP-OES technique. The content of Ni in the NiO/palygorskite composites is about 16.75 wt%, and thereby, the content NiO in the composite is approximate 20.86 wt%.

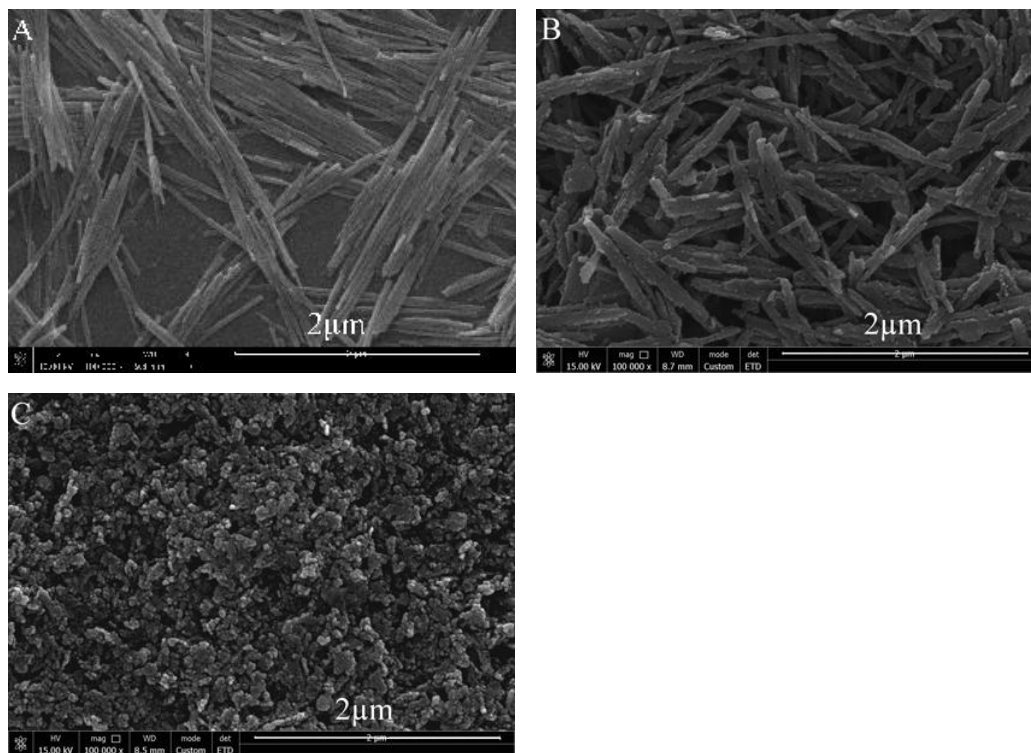


Figure 2. SEM images for palygorskite (A), NiO/palygorskite (B) and as-prepared NiO nanoparticles (C).

To investigate the morphologies of the obtained materials, SEM and TEM measurement were performed and shown in Fig. 2 and 3. Fig. 2 shows the SEM images of palygorskite, NiO nanoparticles and NiO/palygorskite composites. The palygorskite (Fig. 2A) exhibited the bundles of fibrous structures, and the single fiber of palygorskite had smooth surface with diameter of about 40 – 60 nm and length of about 0.7 – 1.8 μm. In NiO/palygorskite composites, irregular congregated nanoparticles were covered on the surface of palygorskite nano fibers, and the diameter of NiO/palygorskite became to about 45 – 75 nm, as depicted in Fig. 2B. The morphologies of the obtained NiO nanoparticles present irregular congregated nanoparticles, and the size of individual nanoparticle is the range of 30 – 75 nm, as shown in Fig. 2C.

The TEM images of palygorskite, NiO/palygorskite composites and the as-prepared NiO nanoparticles are shown in Fig. 3. Comparing with the original palygorskite (Fig. 3A), the surface morphologies of NiO/palygorskite composites had obviously changed. There are lots of ultrafine particles loaded on to the interface of palygorskite, which could be confirmed in Fig. 3B. These results directly demonstrate that the NiO/palygorskite composites have been successfully synthesized, and the NiO particles are well dispersed on the surface of palygorskite, which is accorded with the results of SEM images. The TEM image shown in Fig. 3C indicates the aggregation of the as-prepared NiO.

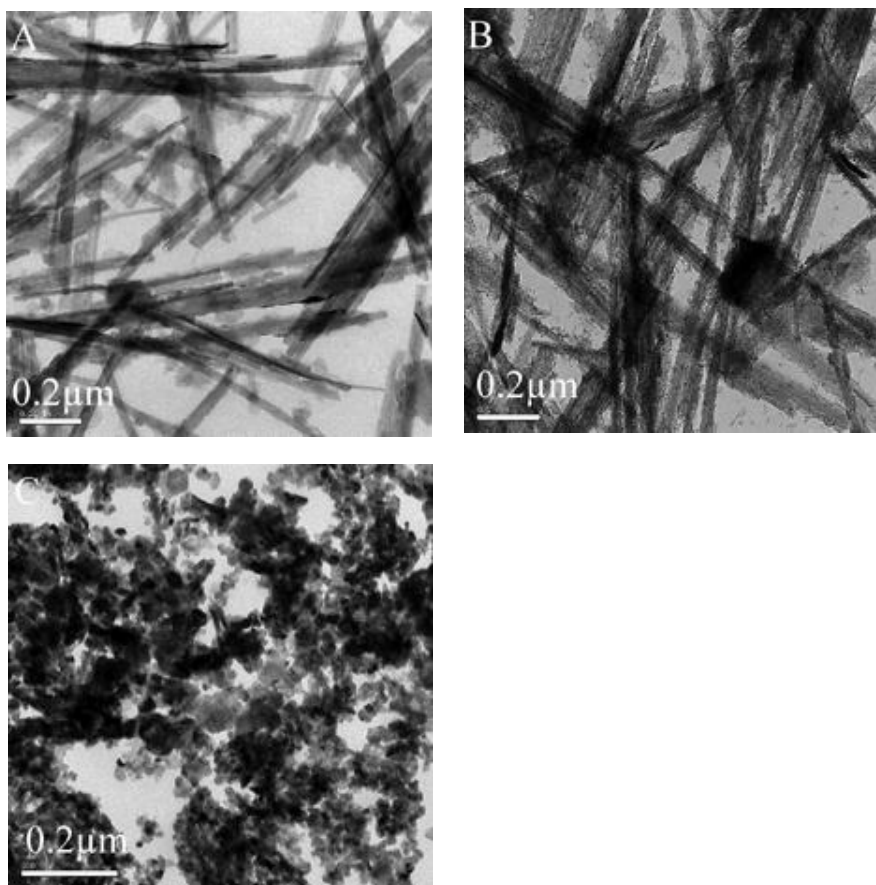


Figure 3. TEM images for palygorskite (A), NO/palygorskite (B) and as-prepared NiO nanoparticles (C)

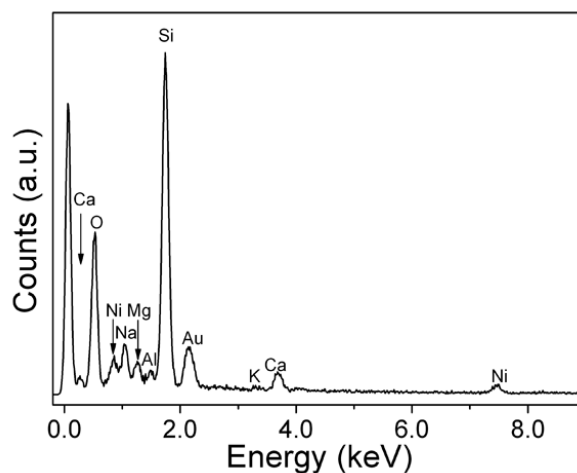


Figure 4. EDS spectrum of NiO/palygorskite composite.

The chemical composition of the NiO/palygorskite composites is also determined by EDS technique and shown in Fig. 4. Only those peaks with the elements of Na, K, Ca, Mg, Al, Si, Ni, O and Au are present in the EDS spectrum, the peaks of Na, K, Ca, Mg, Al and Si are come from palygorskite and the of the Au peaks arise from the gold sputtered on the sample surface. This result

also confirmed that NiO/palygorskite composites have been successfully synthesized. The content of Ni in the NiO/palygorskite composites is about 15.24 wt%, and thereby, the content NiO in the composite is approximate 19.39 wt%, which is approximate to the ICP-OES result.

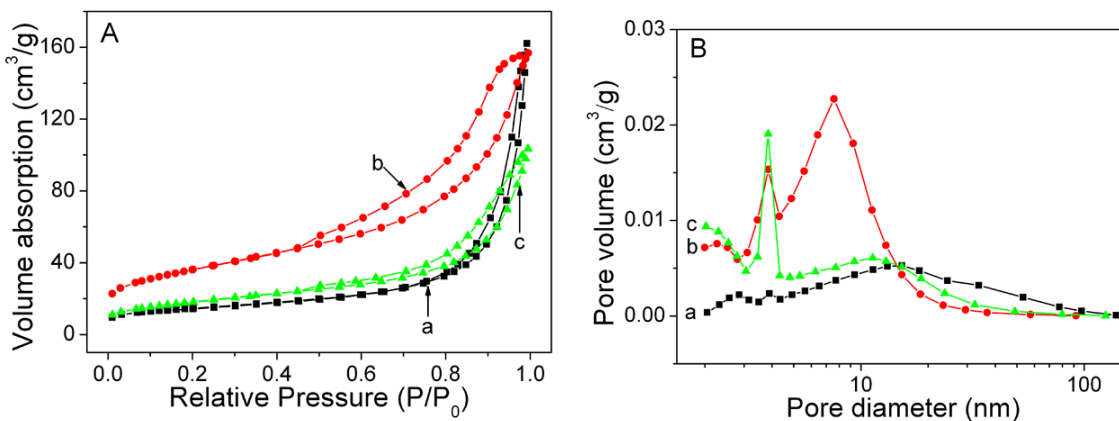


Figure 5. BET isotherms (A) and BJH pore size distribution (B) of palygorskite (curve a), NiO/palygorskite (curve b) and as-prepared NiO nanoparticles (curve c).

BET specific surface area and the BJH pore size distribution of palygorskite, NiO/palygorskite composites and NiO nanoparticles have been measured. Fig. 5A shows the nitrogen adsorption/desorption isotherm of palygorskite, Ni(OH)₂/palygorskite and NiO/palygorskite composites. A small hysteresis loop at high relative pressure region (>0.9 P/P₀) indicates the macroporosity of the obtained palygorskite (curve a). The mesoporous nature of Ni(OH)₂/palygorskite and NiO/palygorskite composites are proved by the irreversible type IV adsorption/desorption isotherm, as shown in curve b and c. The BET surface area of the palygorskite, Ni(OH)₂/palygorskite and NiO/palygorskite composites are 51.4, 65.6 and 129.2 m²/g, respectively. The surface area of the obtained NiO/palygorskite composite is larger than that of ZnO-NiO composite [25]. The BJH pore size distribution of the above materials is shown in Fig. 5B. The palygorskite has a broad pore distribution of 2 – 140 nm (curve a). Under the decomposition of 350 °C for 6 hours, the prepared NiO/palygorskite composites have a narrow mesopore size distribution at around 3.8 and 7.6 nm (curve b). The pores of 3.8 nm may result from the calcination of Ni(OH)₂ and the pores of 7.6 nm probably come from the synergetic effect of palygorskite. The pore distribution of obtained NiO nanoparticles is in the range of 3 - 40 nm, and centered at 3.8 nm. The average pore diameter of this material is about 9.7 nm (curve c). Note that the ion transfer rate in a porous system, and the extent of electrode/electrolyte interfacial area, are determined by the porosity of the electrode material, thereby, the porous structure and high surface area of the electrode material are beneficial to supercapacitor performance. Therefore, the NiO/palygorskite composite is expected to exhibit good supercapacitor performance.

The electrochemical performances of the obtained NiO/palygorskite composite and as-prepared NiO were firstly evaluated through CV measurements in the potential range of -0.1 to 0.6 V at scan rates of 2, 5, 10 and 20 mV/s, and the electrolyte is 2.0 mol/L KOH. As shown in Fig. 6, at different

scan rates, a couple of redox peaks can be observed and the peak currents are linearly proportional to the scan rate, suggesting that the capacity mainly results from pseudocapacitive capacitance, which is based on a redox mechanism [26]. For nickel oxide as an electrode active material, it is well accepted that the surface Faraday reaction can be expressed as follows:



The C_s values can be calculated from the CV curves by using the following equation:

$$C_s = \frac{1}{vm} \int_{V_i}^{V_f} i dV \quad (2)$$

where C_s (F/g) is specific capacitance, m is the mass of NiO/palygorskite composite (g), i the cathodic or anodic current (A) in the potential range of V_i to V_f .

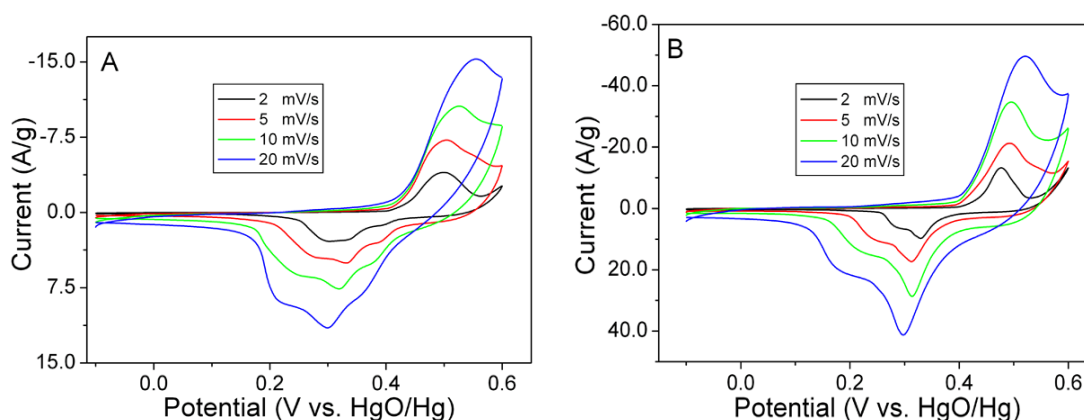


Figure 6. CV curves of NiO/palygorskite composite (A) and as-prepared NiO nanoparticles (B) at different scan rates.

The specific capacitances of the NiO/palygorskite composite could be calculated from Fig. 6A, and they are 197.1, 172.1, 129.9 and 89.0 F/g, when the scan rates are 2, 5, 10 and 20 mV s^{-1} , respectively. From the ICP-OES result, the content of NiO in the NiO/palygorskite composite is 20.86 wt%, so, the C_s values in NiO are 944.8, 824.8, 622.7 and 426.8 F/g, correspondingly. The C_s value of NiO in NiO/palygorskite composite is a bit less than that of ZnO-NiO composite [25], and the possible reason may be the bad conductivity of palygorskite. For the as-prepared NiO (Fig. 6B), the corresponding C_s values 503.2, 483.1, 443.9 and 334.0 F/g, respectively. The high specific capacitance value of NiO in the NiO/palygorskite composite can be attributed to their higher specific surface area and proper pores, which provide effective diffusion channels for the electrolyte ions leading to an improved pseudocapacitive performance. However, the C_s value of NiO in the NiO/palygorskite dropped more sharply than that of bare NiO, which could be contributed to the lower conductivity of NiO/palygorskite.

The accurate specific capacitance of NiO in the NiO/palygorskite composite is calculated from the galvanostatic discharge curves based on the following equation:

$$C_s = \frac{i \times \Delta t}{\Delta V} \quad (3)$$

where i is the discharge current density (discharge current divided by the mass of NiO/palygorskite

composite), Δt is the duration for a full discharge, and ΔV is the voltage change after a full discharge. As shown in Fig. 7A, when the discharge current density are 2.0, 1.0, 0.5 and 0.25 A/g, the corresponding C_s values of NiO/palygorskite composite are 110.0, 157.8, 132.5, 198.6 and 226.4 F/g, respectively. The C_s values calculated in NiO are calculated to be 527.3, 756.5, 952.1 and 1085.3 F/g, correspondingly. For the as-prepared NiO, the corresponding C_s values calculated from Fig. 7B are 503.2, 483.1, 443.9 and 334.0 F/g, respectively. These results are approximate to the CV results.

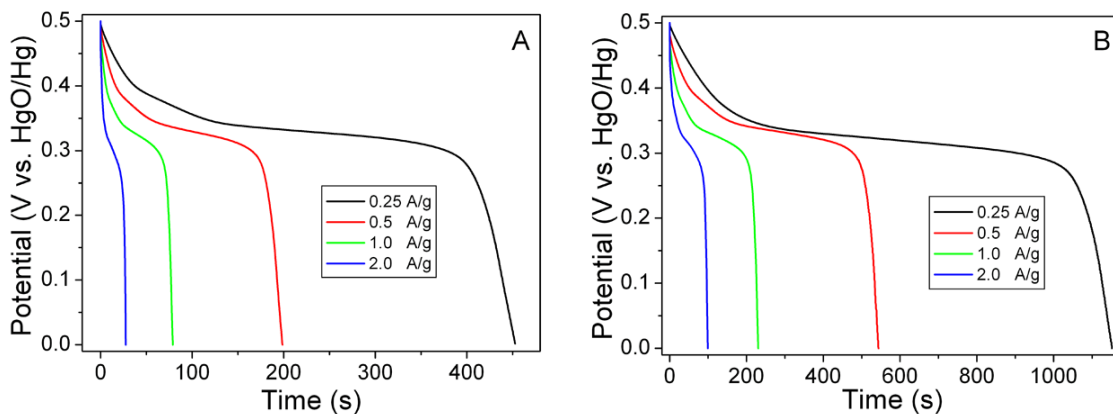


Figure 7. Discharge curves NiO/palygorskite composite (A) and as-prepared NiO nanoparticles (B) at different discharge current densities.

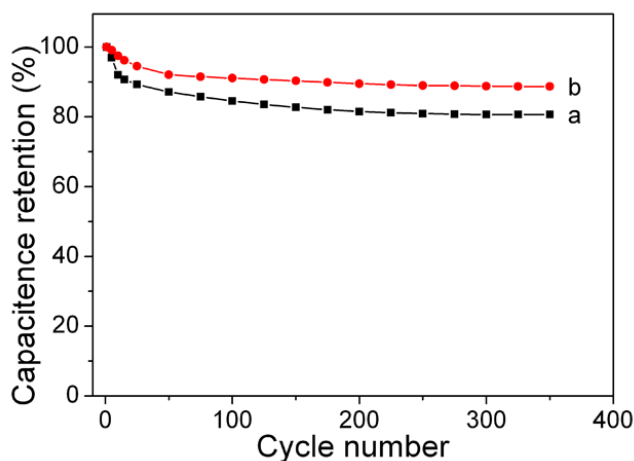


Figure 8. Cycling performance of NiO/palygorskite composite (curve a) and as-prepared NiO nanoparticles (curve b) electrodes at the current density of 1.0 A/g in 2.0 mol/L KOH electrolyte.

The cyclic stability of the electrode material is very important for practical applications. The NiO/palygorskite composite and as-prepared NiO electrodes were employed in charge/discharge test at current density of 1.0 A/g up to 350 cycles. Fig. 8 shows the profile of capacitance retention with number of cycles. Even after 350 continuous charge/discharge cycles the NiO/palygorskite composite retains 80.6% of the initial capacitance (curve a), but the NiO possesses 88.7% of its initial capacitance

(curve b). The cyclic stability of NiO/palygorskite is not as satisfy as composites such as ZnO-NiO, Ni-Co oxides on TiO₂ tubes and nickel-cobalt layered double hydroxides on zinc tin oxides [25, 27, 28], which could be contributed to the lower conductivity of NiO/palygorskite.

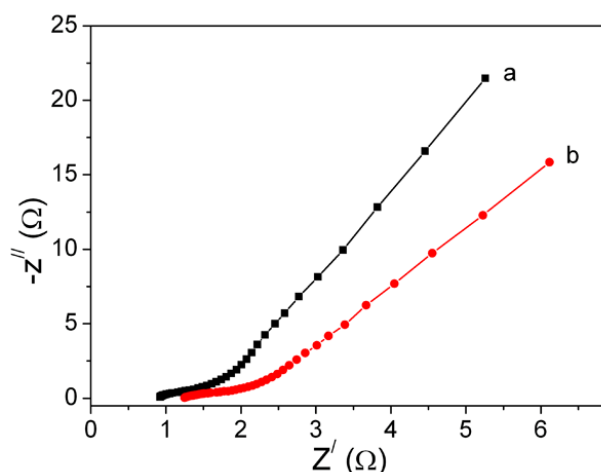


Figure 9. Ragone plot of the as-prepared NiO nanoparticles (curve a) and NiO/palygorskite composite (curve b).

Fig. 9 shows the Nyquist plot of NiO/palygorskite composite and the as-prepared NiO materials at the potential of 0.5 V with a frequency range from 10⁵ to 0.01 Hz in 2.0 mol/L KOH aqueous solution, Z' and Z'' are the real and imaginary parts of the impedance, respectively. The plot is composed of a distorted semicircle like plateau at high frequency region and a line at low-frequency region. The plateau is due to the charge transfer in Faraday reactions, and the straight line is related to the diffusion of ions in the materials bulk. Compared with Nyquist plot of the as-prepared NiO (curve a), the NiO/palygorskite composite (curve b) has a larger diameter of distorted semicircle, which means higher charge transfer resistance because of the lower conductivity of NiO/palygorskite composite. The straight line in the Nyquist plot of NiO/palygorskite composite is lower than that of the as-prepared NiO, which indicates improved electrolyte diffusion in the materials.

4. CONCLUSIONS

NiO/palygorskite composites were successfully fabricated through hydrothermal combined calcination methods. Due to the high disperse of NiO on the surface of palygorskite, the obtained NiO/palygorskite composite has high surface area with a bimodal mesopore size distribution at around 3.8 and 7.6 nm. Contributed to its high surface area and proper pore size distribution, NiO in the NiO/palygorskite composites can exhibit maximum specific capacitance of 1085.3 F/g at current density of 0.25 A/g. But the low conductivity of the NiO/palygorskite composites restricts its charge/discharge cycling property (maintained about 80.6 % at 1.0 A/g after 350 cycles). Adding another material to improve its conductivity maybe a good choice, and this research is in progress.

ACKNOWLEDGMENTS

This work was partially supported by the Industrial Support Project of Huaian of Jiangsu Province (HAG 2012003), the overseas training project of Jiangsu Province for outstanding young teachers and principals in colleges, and the College Natural Science Foundation of Jiangsu Province (13KJB530002).

References

1. D. Wang, W. Ni, H. Pang, Q. Lu, Z. Huang, J. Zhao, *Electrochim Acta*, 55 (2010) 6830 - 6835.
2. X. Zhang, W. Shi, J. Zhu, W. Zhao, J. Ma, S. Mhaisalkar, T.L. Maria, Y. Yang, H. Zhang, H.H. Hng, Q. Yan, *Nano Res.*, 3 (2010) 643 - 652.
3. X. Xia, J. Tu, X. Wang, C. Gu, X. Zhao, *J. Mater. Chem.*, 21 (2011) 671 - 679
4. J. Li, W. Zhao, F. Huang, A. Manivannanc, N. Wu, *Nanoscale*, 3 (2011) 5103 - 5109.
5. Z. Lu, Z. Chang, J. Liu, X. Sun, *Nano Res.*, 4 (2011) 658 - 665.
6. D. Su, H.S. Kim, W.S. Kim, G. Wang, *Chem. Eur. J.*, 18 (2012): 8224 - 8229.
7. Y.Q. Zhang, X.H. Xia, J.P. Tu, Y.J. Mai, S.J. Shi, X.L. Wang, C.D. Gu, *J. Power Sources*, 199 (2012) 413 - 417.
8. S. Vijayakumar, S. Nagamuthu, G. Muralidharan, *ACS Appl. Mater. Interfaces*, 5 (2013) 188 - 2196.
9. K. Liang, X. Tang, W. Hu, *J. Mater. Chem.*, 22 (2012) 11062 - 11067.
10. X. Li, S. Xiong, J. Li, J. Bai, Y. Qian, *J. Mater. Chem.*, 22 (2012) 14276 - 14283.
11. H. Cha, X. Chen, D. Jia, S. Bao, W. Zhou, *Mater. Res. Bull.*, 47 (2012) 3947 - 3951.
12. H. Pang, Y. Shi, J. Du, Y. Ma, G. Li, J. Chen, J. Zhang, H. Zheng, B. Yuan, *Electrochim. Acta*, 85 (2012) 256 - 262.
13. S.I. Kim, J.S. Lee, H.J. Ahn, H.K. Song, J.H. Jang, *ACS Appl. Mater. Interfaces*, 5 (2013) 1596 - 1603.
14. G. Wang, L. Liu, L. Zhang, J. Zhang, Nickel, *Ionics*, 19 (2013) 689 - 695.
15. F. Gao, Q. Wei, J. Yang, H. Bi, M. Wang, *Ionics*, 19 (2013) 1883 - 1889.
16. D. Wang, Q. Wang, T. Wang, *Ionics*, 19 (2013) 559 - 570.
17. Y. Yang, J. He, Y. Gu, D. Li, L. Zhu, J. Chen, X. Li, L. Feng, *Synth. React. Inorg. M.*, 43 (2013) 296 - 304.
18. L. Feng, Y. Zhu, H. Ding, C. Ni, *J. Power Sources*, 267 (2014) 430 - 444.
19. Q. Lu, J.G. Chen, J.Q. Xiao, *Angew. Chem. Int. Ed.*, 52 (2013) 1882 - 1889.
20. S. Ardizzone, G. Frengonara, S. Trasatti, *Electrochim. Acta*, 35 (1990) 263 - 267.
21. H. Jiang, J. Ma, C. Li, *Adv. Meter.*, 24 (2012) 4197 - 4202.
22. C. Huo, H. Yang, *J. Colloid Interf. Sci.*, 384 (2012) 55 - 60.
23. S. Miao, Z. Liu, Z. Zhang, B. Han, Z. Miao, K. Ding, G. An, *J. Phys. Chem. C*, 111 (2007) 2185 - 2190.
24. L.L. Zhang, F.J. Lv, W.G. Zhang, R.Q. Li, H. Zhong, Y.J. Zhao, Y. Zhang, X. Wang, *J. Hazard Mater.*, 171 (2009) 294 - 300.
25. H. Pang, Y. Ma, G. Li, J. Chen, J. Zhang, H. Zheng, W. Du, *Dalton Trans.*, 41 (2012) 13284 - 13291.
26. K.C. Liu, M.A. Anderson, *J. Electrochem. Soc.*, 143 (1996) 124 - 130.
27. F. Yang, J. Yao, F. Liu, H. He, M. Zhou, P. Xiao, Y. Zhang, *J. Mater. Chem. A*, 1 (2013) 594 - 601.
28. X. Wang, A. Sumbaja, M. Lin, J. Yan, P. S. Lee, *Nanoscale*, 4 (2012) 7266 - 7272.